ADVANCES IN ATMOSPHERIC SCIENCES, VOL. 36, AUGUST 2019, 779–792

• **Original Paper** •

Influence of Intraseasonal Oscillation on the Asymmetric Decays of El Niño and La Niña

Xiaomeng SONG[1], Renhe ZHANG*[2], and Xinyao RONG[1]

[1]*State Key Laboratory of Severe Weather, Chinese Academy of Meteorological Sciences, Beijing* 100081*, China*

[2]*Department of Atmospheric and Oceanic Sciences and Institute of Atmospheric Sciences, Fudan University, Shanghai* 200433*, China*

(Received 8 February 2019; revised 17 April 2019; accepted 30 April 2019)

ABSTRACT

Warm and cold phases of El Niño–Southern Oscillation (ENSO) exhibit a significant asymmetry in their decay speed. To explore the physical mechanism responsible for this asymmetric decay speed, the asymmetric features of anomalous sea surface temperature (SST) and atmospheric circulation over the tropical Western Pacific (WP) in El Niño and La Niña mature-to-decay phases are analyzed. It is found that the interannual standard deviations of outgoing longwave radiation and 850 hPa zonal wind anomalies over the equatorial WP during El Niño (La Niña) mature-to-decay phases are much stronger (weaker) than the intraseasonal standard deviations. It seems that the weakened (enhanced) intraseasonal oscillation during El Niño (La Niña) tends to favor a stronger (weaker) interannual variation of the atmospheric wind, resulting in asymmetric equatorial WP zonal wind anomalies in El Niño and La Niña decay phases. Numerical experiments demonstrate that such asymmetric zonal wind stress anomalies during El Niño and La Niña decay phases can lead to an asymmetric decay speed of SST anomalies in the central-eastern equatorial Pacific through stimulating different equatorial Kelvin waves. The largest negative anomaly over the Niño3 region caused by the zonal wind stress anomalies during El Niño can be threefold greater than the positive Niño3 SSTA anomalies during La Niña, indicating that the stronger zonal wind stress anomalies over the equatorial WP play an important role in the faster decay speed during El Niño.

Key words: ENSO, asymmetry, ENSO decay, intraseasonal oscillation, OGCM

Citation: Song, X. M., R. H. Zhang, and X. Y. Rong, 2019: Influence of intraseasonal oscillation on the asymmetric decays of El Niño and La Niña. *Adv. Atmos. Sci.*, **36**(8), 779–792, https://doi.org/10.1007/s00376-019-9029-6.

Article Highlights:

- Warm and cold phases of ENSO exhibit a significant asymmetry in their decay speed.
- The difference in intraseasonal oscillation intensity bring about the asymmetry of zonal wind anomalies over the equatorial WP during El Niño and La Niña decay phases.
- The asymmetric zonal wind anomalies over the equatorial WP result in asymmetry in El Niño and La Niña decay phases.

1. Introduction

Many studies have revealed that asymmetry exists between warm and cold phases of the El Niño–Southern Oscillation (ENSO). Previous studies have proposed a variety of mechanisms about the causes of ENSO amplitude asymmetry, including the asymmetric atmospheric response to sea surface temperature anomalies (SSTAs) (Kang and Kug, 2002), the oceanic nonlinear dynamical heating (An and Jin, 2004; Su et al., 2010), the asymmetric heating of tropical instability waves (An, 2008), and biological–physical feedback (Timmermann and Jin, 2002), as well as the nonlinear rectification of the low-frequency surface wind stress by the high-frequency wind anomalies (Rong et al., 2011).

In addition to the amplitude asymmetry, the characteristics of the evolution of El Niño and La Niña events during their decay phases are markedly different (Kessler, 2002; Larkin and Harrison, 2002; McPhaden and Zhang, 2009). Generally, El Niño events tend to turn into La Niña events in the following June–July after their mature phases; however, the negative SSTAs associated with La Niña events can persist for more than one year after peaking, and tend to strengthen again in the next winter (Okumura and Deser, 2010; Okumura et al., 2011), resulting in a longer duration than that of El Niño. DiNezio and Deser (2014) pointed out that a large fraction (35%–50%) of La Niña events can sustain for more than two years. Such remarkable differences between the characteristics of the evolution of La Niña and El Niño thus challenges traditional ENSO cycle theories (Suarez

* Corresponding author: Renhe ZHANG
Email: rhzhang@fudan.edu.cn

and Schopf, 1988; Battisti and Hirst, 1989; Jin, 1997) and ENSO forecast (Jin and Kinter III, 2009; Ohba and Watanabe, 2012).

The evolution of ENSO is tightly connected with the zonal wind stress anomalies over the equatorial western Pacific (WP). Zhang and Huang (1998) pointed out that the intensity of the zonal wind stress anomalies over the equatorial WP are closely related to the termination of ENSO, because the anomalous easterly over the equatorial WP during the mature phase of El Niño can stimulate cold equatorial Kelvin waves by upwelling and cooling, leading to the transition from El Niño to La Niña (Huang et al., 2001; Yan et al., 2001). Ohba and Ueda (2009) suggested that the distinct characteristics of evolution between El Niño and La Niña decay phases are mainly due to the different distributions of zonal wind stress anomalies over the equatorial WP between ENSO warm and cold phases. During an El Niño mature phase, the evident easterly anomalies in the equatorial WP can induce eastward cold Kelvin waves that eliminate the positive SSTAs in the central-eastern equatorial Pacific (CEEP), leading to the phase transition from El Niño to La Niña. However, during La Niña the westerly anomalies are considerably weaker, and thus the resulting downwelling Kelvin waves cannot counteract the negative SSTAs in the CEEP, meaning La Niña can persist for longer compared with El Niño. The authors argued that the nonlinear response of atmospheric deep convection to SSTAs is the main reason for the distinct anomalous zonal wind over the equatorial WP between El Niño and La Niña (Hoerling et al., 1997; Kang and Kug, 2002; Okumura et al., 2011; Dommenget et al., 2013). During La Niña, the anomalous precipitation center shifts westward by about 10°–15° relative to that of El Niño. Therefore, the easterly anomalies associated with negative precipitation anomalies will efficiently reduce the westerly anomalies over the equatorial WP during La Niña, resulting in an asymmetric distribution of zonal wind anomalies over the equatorial WP between El Niño and La Niña mature phases.

Except for the asymmetry of zonal wind anomalies, the southward shift of westerlies during El Niño is considered favorable for its termination (Harrison and Vecchi, 1999), which can change the zonal mean equatorial heat content (HC) and establish a meridional asymmetry of thermocline depth in the turnaround phase of ENSO, leading to a durational asymmetry between El Niño and La Niña (McGregor et al., 2012; Abellán and McGregor, 2016). In addition to atmospheric asymmetric processes, oceanic processes can play a role in prolonging La Niña. Nagura et al. (2008) showed that tropical instability waves slow the transition from La Niña to El Niño. Hu et al. (2014) considered that reflected Rossby waves may interrupt the recharge process and prevent the transition from La Niña to El Niño. DiNezio and Deser (2014) proposed that nonlinearity in the delayed thermocline feedback is the sole process prolonging the duration of La Niña in a nonlinear delayed-oscillator model.

The zonal wind anomalies over the equatorial WP during ENSO mature phases are tightly linked to an anomalous low-level western North Pacific (WNP) anticyclone (WNPAC) and cyclone (WNPC) (Zhang et al., 1996, 2017; Wang et al., 1999; Li et al., 2017). The easterly anomalies located in the south wing of the WNPAC during an El Niño mature phase can extend southward to the equatorial WP, which is conducive to motivating cold equatorial Kelvin waves; while a westward shifting NWPC during La Niña leads to a weaker equatorial thermocline anomaly, which acts as a weaker dynamic forcing to produce a weaker effect on SSTAs, bringing about a longer duration of La Niña that persists to the next year (Chen et al., 2016; Tao et al., 2017). It is suggested that Indian Ocean SSTAs may partially contribute to the occurrence of zonal wind anomalies over the equatorial WP during ENSO mature-to-decay phases (Ohba and Ueda, 2009; Okumura and Deser, 2010; Ohba and Watanabe, 2012). The atmospheric Kelvin wave response to warming in the Indian Ocean basin can induce easterly anomalies over the equatorial WP and enhance the low-level anticyclone (Xie et al., 2009; Okumura et al., 2011); nevertheless, it has been noted that the role of Indian Ocean basin warming is more pronounced in the summer of decaying El Niño events.

Zhang et al. (2015) pointed out that the intraseasonal oscillation over the WNP is weak and the interannual variation dominates the wind variability during El Niño winters; whereas, during La Niña winters the intraseasonal oscillation is dominant and the interannual variation is weak. Such a difference leads to much stronger anomalous anticyclones during El Niño than the anomalous cyclones during La Niña, causing an asymmetric effect on the precipitation over southern China. The SSTAs over the tropical WP play a crucial role in the different intensities of atmospheric intraseasonal variability between El Niño and La Niña. The Walker circulation can be affected by the zonal gradient of SSTAs and changes in atmospheric convection are a clue to the Walker circulation slowdown (Tokinaga et al., 2012). Negative SSTAs during El Niño can weaken the zonal gradient of SSTAs and lead to a stronger anomalous anti-Walker circulation, resulting in anomalous descending motion and convective cooling over the tropical WP, which is unfavorable for the development of atmospheric intraseasonal oscillation. Meanwhile the reverse is true during La Niña (Gao et al., 2018).

The study of Zhang et al. (2015) mainly focused on the asymmetry of atmospheric circulation during the wintertime of ENSO years, i.e., the mature and decay phases of ENSO. Thus, a question arises: can the distinct intensity of intraseasonal oscillation between El Niño and La Niña influence the asymmetry of zonal wind anomalies over the equatorial WP during ENSO mature-to-decay phases, and consequently lead to asymmetric decays in El Niño and La Niña? To address this, the present study begins with an analysis of the anomalous distributions and asymmetric characteristics of SSTAs and atmospheric circulation anomalies during El Niño and La Niña mature-to-decay phases, based on observation data. Then, we discuss the relationship between the asymmetric characteristics of wind anomalies and intraseasonal variability. Finally, numerical experiments are performed using a

global ocean general circulation model (OGCM) to investigate the contribution of zonal wind anomalies over the equatorial WP to the CEEP SSTAs during El Niño and La Niña decay phases.

2. Data, model and methods

2.1. *Data and analysis method*

The sea level pressure (SLP), 850 hPa wind, and surface wind stress utilized in this study are from the ERA-Interim dataset, with a resolution of $1^\circ \times 1^\circ$ (Dee et al., 2011). The SST data are from HadISST, with a $1^\circ \times 1^\circ$ horizontal resolution (Rayner et al., 2003). The outgoing longwave radiation (OLR) is derived from NOAA/AVHRR data, with a $2.5^\circ \times 2.5^\circ$ horizontal resolution (Liebmann and Smith, 1996). The surface air temperature, SST, and specific humidity used in the model are from COADS (Da Silva et al., 1994). Except for the COADS data that used in the model, the period of other data is from 1979 to 2016, and an anomaly is defined as the departure from the seasonal cycle averaged over this period. In this study, the intraseasonal component is obtained using Lanczos bandpass filtering (10–50 days), and the interannual component is calculated using a three-month running mean based on monthly anomalies.

As in Zhang et al. (2015), the criteria for selecting ENSO events is as follows: if the averaged SSTA over the Niño3 region (150°–90°W, 5°S–5°N) in a winter half year (November to April) is greater (less) than 0.5°C, then the winter half year is considered as an El Niño (La Niña) episode. Eight El Niño events (1982/83, 1986/87, 1991/92, 1994/95, 1997/98, 2002/03, 2009/10, 2015/16) and ten La Niña events (1984/85, 1985/86, 1988/89, 1995/96, 1998/99, 1999/00, 2005/06, 2007/08, 2010/11, 2011/12), are identified based on these criteria during 1979–2016.

2.2. *Model and experiments*

The model used in this study is the Modular Ocean Model, version 3, developed by the Geophysical Fluid Dynamics Laboratory (Pacanowski and Griffies, 1999). This model adopts a realistic topography, with the model domain ranging from 77°S to 65°N meridionally and reaching down to 5300 m vertically. The horizontal resolution is $1^\circ \times 1^\circ$, with the meridional resolution varying densely to 1/3° around equator. There are 35 vertical levels, with 20 even levels above 300 m and a 10 m thickness for the uppermost layer. The model adopts a barotropic–baroclinic time splitting algorithm and the explicit free surface scheme is used in this study. Physical parameterizations include the K-Profile Pacanowski–Philandar vertical mixing scheme, the isoneutral mixing scheme, and shortwave solar penetration. To remove the restoration effect of surface air temperature and specific humidity on SST, in this study we use the algorithm of Rong et al. (2011) to calculate the sensible and latent heat fluxes by bulk formula. The surface air temperature (T_a) and specific humidity (q_a) are derived by empirical formulas according to the SSTA:

$$T_a = T_{ac} + \alpha(x,y)\Delta T_s \,, \tag{1}$$

$$q_a = q_{ac} + \beta(x,y)\Delta T_s \,, \tag{2}$$

where T_s is the observed SST and $\Delta T_s = T_s - T_{sc}$; and T_{ac}, T_{sc} and q_{ac} are the observed climatological surface air temperature, SST and specific humidity, respectively. The coefficients $\alpha(x,y)$ and $\beta(x,y)$ vary with space and are calculated by regressing the observed monthly SST anomaly onto the monthly specific humidity and surface air temperature anomaly fields at each grid point. Here, the climatological mean wind speed is derived from COADS, while the wind stress and net shortwave and downward longwave flux are derived from ERA-Interim. In this study, the model sea surface salinity (SSS) is simply restored to the Levitus climatological SSS (Levitus, 1982) with a timescale of 30 days.

The model is initiated from a resting ocean. The initial temperature and salinity are derived from the January climatology of Levitus. First, the model is spun up for 50 years, forced by climatological wind speed, wind stress, and net shortwave and downward longwave radiation, with a Newtonian damping term applied to the model SST by forcing it toward the Levitus climatology. The last 20 years' Newtonian damping terms are then averaged and used as the "flux correction" terms in an additional 50-year spin up run. Therefore, the first 100 years' integration is sufficient to make the model upper ocean reach a quasi-equilibrium state. Starting from the above 100-year spin up integration, a further 10-year integration, using the same forcing as the last 50-year spin up integration, is performed and regarded as the control experiment. Then, four sensitivity experiments are conducted starting from the same initial condition as the control experiment. All the forcing fields between the control and sensitivity experiments are the same, except the zonal wind stress. In this respect, an anomalous zonal wind stress is superposed onto the climatological wind stress in the sensitivity experiments. Detailed descriptions of the sensitivity experiments are presented in section 5.

3. Asymmetric characteristics of El Niño and La Niña duration

3.1. *SSTA evolution*

ENSO events are characterized by a significant seasonal phase-locking that peaks in winter and decays after the following spring. A common metric used to represent ENSO is the Niño3 index, defined as the averaged SSTA over the Niño3 region (5°S–5°N, 150°–90°W). Figure 1 shows the composite Niño3 index for El Niño and La Niña, respectively. Note that the sign of the Niño3 index for La Niña is reversed to facilitate comparison. The seasonal phase-locking feature of the SSTA during ENSO warm and cold episodes can be clearly observed from Fig. 1. The composite Niño3 index generally peaks in winter and declines from the next spring. Both the amplitude and decay speed of El Niño are noticeably stronger than those of La Niña. The composite Niño3 index of El Niño crosses the zero line and turns into negative values

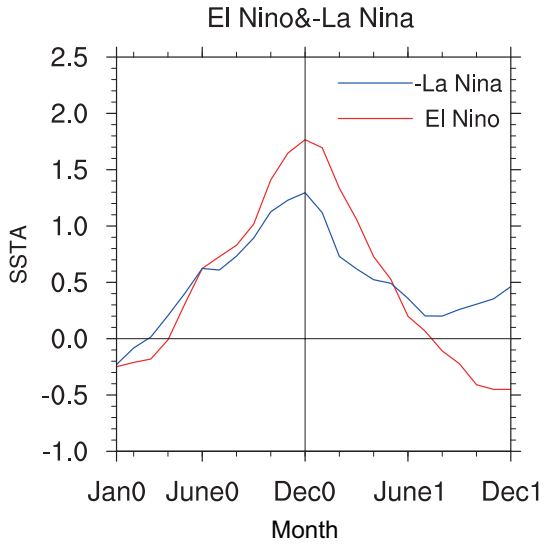

Fig. 1. Composite time series of the Niño3 index (units: °C) for El Niño (red) and La Niña (blue), where the time axis runs from January of the El Niño/La Niña year (Jan0) to December of the following year (Dec1). The Niño3 index for La Niña is multiplied by −1.

around the following July after its peak. However, during the La Niña decay phase the negative SSTA reinforces again after the following summer and tends to develop as a secondary cold event. By calculating the tendency of Niño3 index from January to July of the decay year, it is shown that the averaged decay rate of El Niño Niño3 index is 0.24°C month^{-1}, while that of La Niña is only 0.15°C month^{-1}, indicating an evident asymmetry in decay speed between El Niño and La Niña events.

3.2. *Anomalous atmospheric circulation over the tropical WNP*

Zhang et al. (1996) found that an anomalous anticyclone appears in the lower troposphere over the tropical WNP during El Niño mature phases by compositing the 850 hPa wind anomalies of the 1986/87 and 1991/92 El Niños, and explained it as the atmospheric Rossby wave response to the anomalous convective cooling over the WNP Maritime Continent. Figures 2a and b show the composite SSTAs and 850 hPa wind anomalies over the WNP during El Niño and La Niña mature-to-decay phases, respectively. A pronounced anomalous anticyclone over the WNP during the El Niño mature phase (D0JF1, where D0 represent the December of the mature phase and JF1 represents the January to February of the following year) can be observed in Fig. 2a, with its center located in the east of the Philippines. Moreover, in the equatorial area of its southern wing, prominent easterly anomalies extend from the east Indian Ocean to 150°E latitudinally, and from 10°S to 5°N meridionally. Corresponding to the anomalous anticyclone, a negative SSTA appears in the east of the Philippines, which is responsible for the atmospheric anomalous convective cooling and arouses the anomalous anticyclone. Both the reduction in evaporation induced by northerly anomalies in the east of the WNPAC (Wang et al., 2000) and the oceanic upwelling Rossby waves induced by wind stress curl anomalies on both sides of equator, which corresponds to the westerly anomalies (Wang et al., 1999), are favorable to the generation and maintenance of the negative SSTA over the WNP. The anomalous cyclone over the WNP during the La Niña mature phase is evidently weaker than the anticyclone during El Niño, with warm a SSTA occurring in the east of the Philippines at the same time. Furthermore, westerly anomalies over the south of the anomalous cyclone are remarkably weaker than easterly anomalies over the south of the anomalous anticyclone, the extension of which is smaller too (Fig. 2b). Easterly anomalies over the equatorial WP tend to strengthen and extend eastward to 160°E during the El Niño decay phase (MAM1) (Fig. 2c), whereas the westerly anomalies during La Niña basically remain unchanged (Fig. 2d). Accordingly, both the anomalous anticyclone and its southern easterly anomalies in the mature-to-decay phase (D0JF1 and MAM1) during El Niño are noticeably stronger than the anomalous cyclone and its southern westerly anomalies during La Niña. Because of the critical influence of zonal wind anomalies over the equatorial WP on the decay of ENSO during D0JF1 and MAM1, next we focus mainly on this period and conduct a composite analysis.

The composite SLP and 850 hPa zonal wind anomalies during El Niño and La Niña mature-to-decay phases (D0JFMAM1) are shown in Fig. 3. It is demonstrated in the SLP field (Figs. 3a and b) that there are positive anomalies in the WNP during El Niño, corresponding to the anomalous anticyclone in the lower troposphere. Its maximum center is located in the eastern ocean of the Philippines, with the maximum exceeding 1.4 hPa. The negative anomalies during La Niña are much weaker and located westward compared to the positive anomalies, and its maximum value is only about −1.2 hPa. This indicates that the asymmetry between the intensity of the anomalous anticyclone during El Niño and the anomalous cyclone during La Niña is clearly reflected in the SLP field.

Wu et al. (2010) pointed out that the anomalous anticyclone (anomalous cyclone) over the WNP during ENSO mature phases is closely related to the easterly anomalies (westerly anomalies) over the equatorial WP, and the correlation coefficient between them can reach 0.79. Figure 3c shows the composite 850 hPa zonal wind anomalies during El Niño mature-to-decay phases (D0JFMAM1). The positive anomaly area, which means westerly anomalies, is situated near 20°N over the WP, and easterly anomalies are near the equator, corresponding to the anomalous anticyclone. The pattern during La Niña is almost the opposite (Fig. 3d), corresponding to the anomalous cyclone. Compared with the SLP anomalies, the asymmetry of zonal wind anomalies over the equatorial WP is more pronounced. Easterly anomalies during El Niño are more widely distributed and have a larger central value, the strongest of which can reach −3.1 m s^{-1}; whereas, the extension during La Niña is smaller, with an eastward location and a smaller maximum value (< 2.1

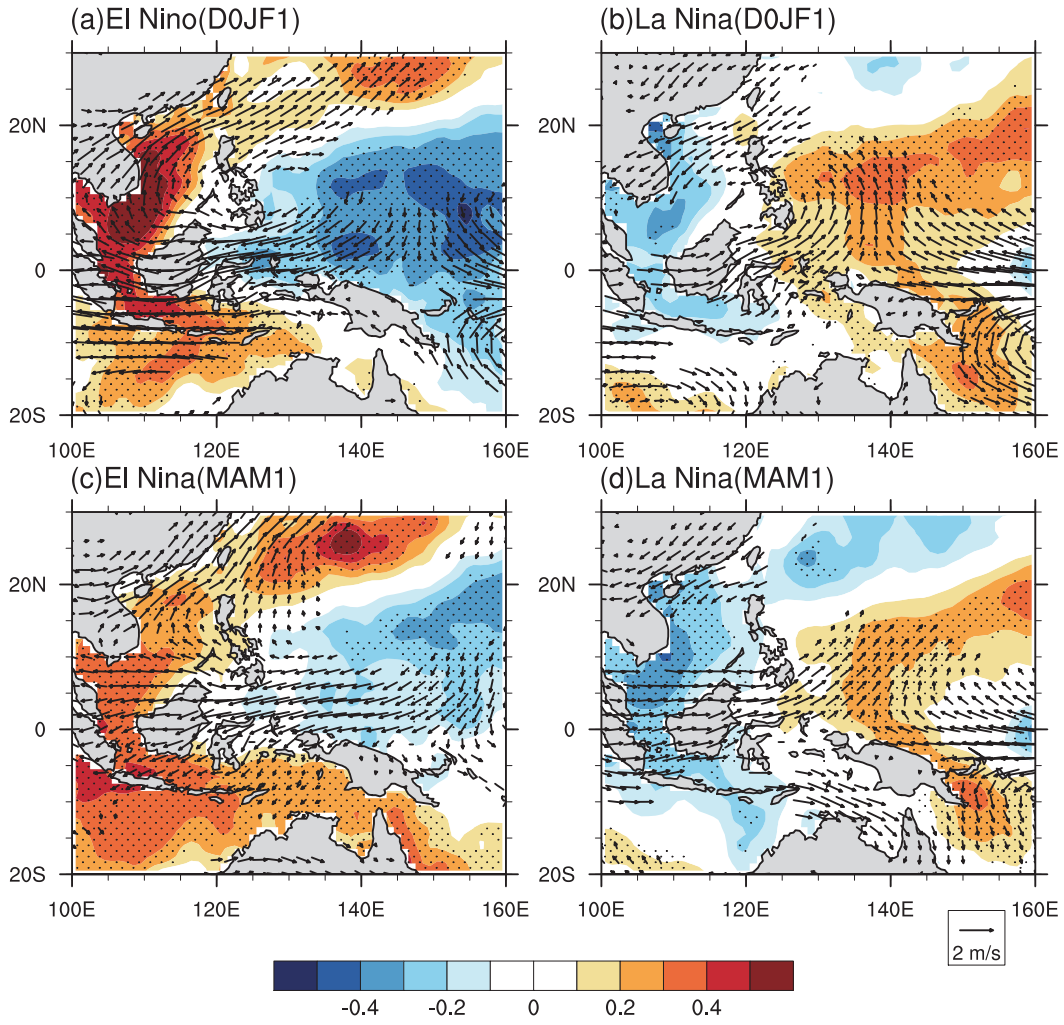

Fig. 2. Composite SSTAs (shading; units: °C) and 850 hPa wind anomalies (vectors; units: m s^{-1}) during (a, c) El Niño and (b, d) La Niña (a, b) mature winter (D0JF1) and (c, d) decay spring (MAM1). Dotted areas and plotted vectors are significant above the 99% confidence level.

m s^{-1}). The situation during ENSO mature phases (D0JF1) is more pronounced, with the maximum values exceeding −3.5 m s^{-1} and 2.3 m s^{-1} for El Niño and La Niña, respectively (figure not shown).

In order to demonstrate the above asymmetries quantitatively, we calculate the regionally averaged values of the three fields according to their high maximum centers, which are shown in Fig. 4. The averaged SSTAs over the WNP key region during El Niño and La Niña (D0JFMAM1) are −0.23°C and 0.19°C, respectively, exhibiting a stronger negative SSTA. Moreover, it is obvious that the anomalous anticyclone is stronger than the anomalous cyclone according to the SLP anomalies (1.11 hPa and −0.94 hPa), which is consistent with the result of Zhang et al. (2015). Nevertheless, the averaged zonal wind anomalies over the key region are −1.23 m s^{-1} for El Niño and 0.69 m s^{-1} for La Niña, and the amplitude of El Niño is around twice as large as that of La Niña, indicating a more pronounced asymmetry in the zonal wind field. Both the SLP and zonal wind anomalies are statistically significant above the 99% confidence level, except the averaged westerly anomalies during La Niña. The above results clearly illustrate that the WNPAC and the associated easterly anomalies near the equator during El Niño are significantly stronger than the WNPC and the westerly anomalies during La Niña.

Figure 5 further shows the temporal evolution of the averaged anomalous 850 hPa zonal winds over the equatorial WP key region during El Niño and La Niña mature-to-decay phases. The Niño3 index is also shown to represent the temporal evolution of ENSO. To facilitate comparison, the sign of zonal wind anomalies is reversed by multiplying by −1. The easterly anomaly around the equator generally appears in the October of an El Niño developing year, and gradually declines after it reaches the maximum value of 1.59 m s^{-1} in December. The evolution of westerly anomalies during La Niña is similar to El Niño but the maximum value is only

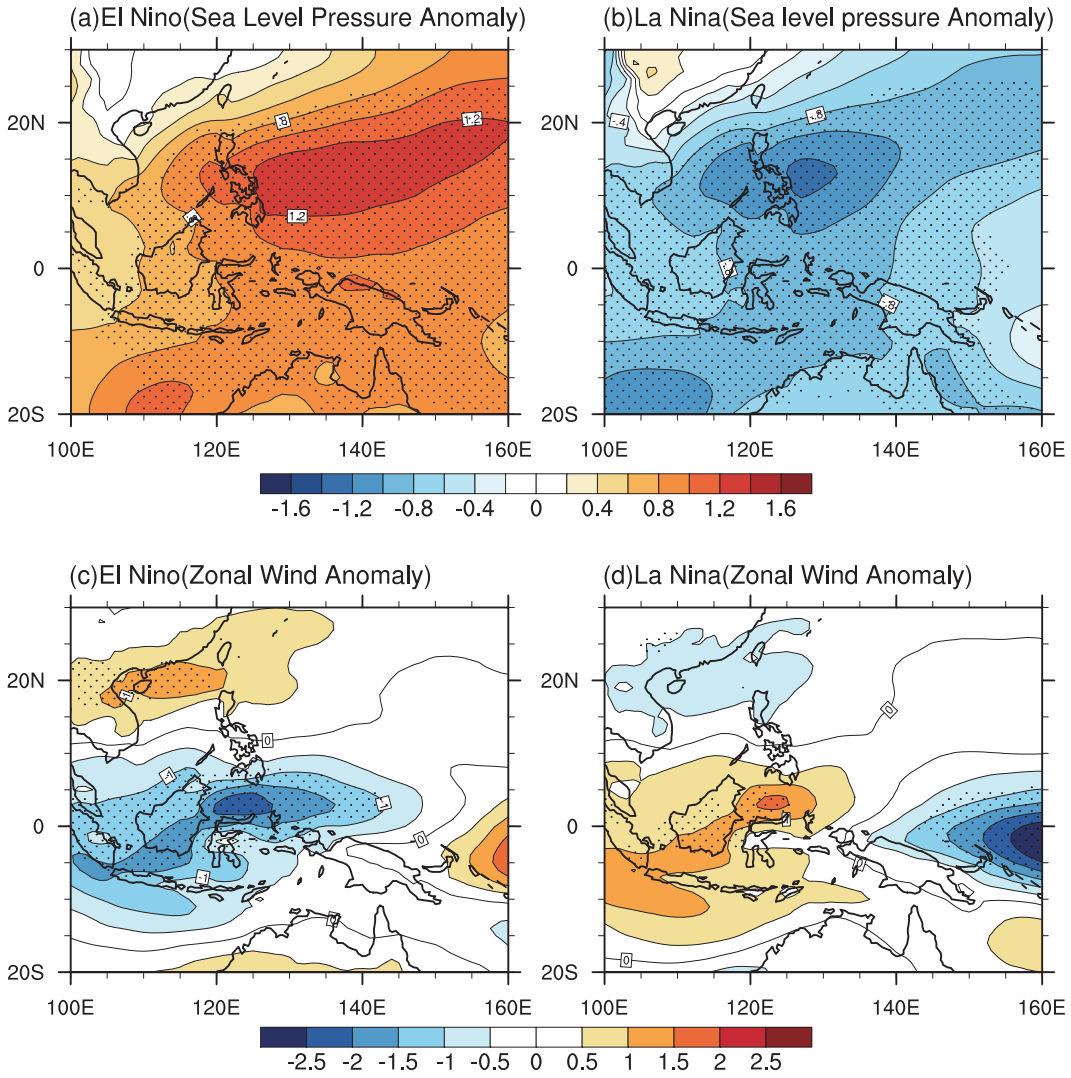

Fig. 3. Composite (a, b) SLP anomalies (units: hPa) and (c, d) 850 hPa zonal wind anomalies (units: m s^{-1}) for (a, c) El Niño and (b, d) La Niña during D0JFMAM1. Dotted areas are significant above the 99% confidence level.

−0.81 m s^{-1}, which is approximately half that of the easterly anomalies' maximum value. The westerly anomalies during La Niña gradually disappear and turn into easterly anomalies in the following June–July, which is favorable for the formation of a secondary cold event; whereas, the easterly anomalies during El Niño can last until the following September and turn into westerly anomalies in October, which seems to be the westerly anomalies in the south of the WNPC during the La Niña following this El Niño.

The strengths of asymmetry are different among the atmospheric and oceanic variables during ENSO mature-to-decay phases. For instance, the ratios of the averaged WNP SSTA and SLP anomalies between El Niño and La Niña are about 1.2–1.3, while those for equatorial zonal wind anomalies can reach 1.78 (Fig. 4) and exceed 2 during the mature phase of ENSO (Fig. 5), implying that the pronounced asymmetry in zonal wind anomalies cannot be merely ascribed to the amplitude asymmetry of the WNP SSTA; instead, it may result from other processes, e.g., the intraseasonal oscillation, which is discussed in the next section.

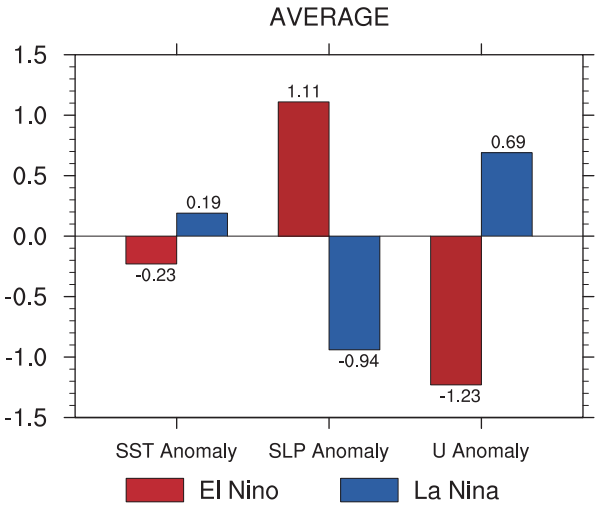

Fig. 4. Regional-averaged SST (0°–20°N, 130°–150°E), SLP (0°–20°N, 120°–150°E) and 850 hPa zonal winds (5°S–5°N, 100°–140°E) anomalies for El Niño (blue) and La Niña (red) during D0JFMAM1.

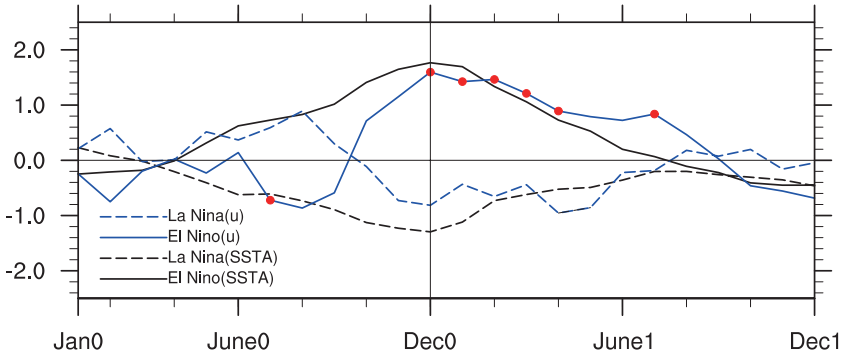

Fig. 5. Composite time series of regional-averaged (5°S–5°N, 100°–140°E) 850 hPa zonal wind anomalies (blue; units: m s^{-1}) and Niño3 index (black; units: °C) for El Niño (solid line) and La Niña (dotted line). The zonal wind anomalies are multiplied by −1. Red dots represent the values exceeding the 95% confidence level.

4. Impact of intraseasonal oscillation

Through comparing the intraseasonal and interannual components of OLR anomalies and kinetic energy anomalies of 850 hPa winds, Zhang et al. (2015) and Li et al. (2015) suggested that the asymmetry in lower tropospheric atmospheric circulation over the WNP between El Niño and La Niña is connected with the different intensities of intraseasonal oscillation during warm and cold phases. Figure 6 shows the distribution of the standard deviations of the OLR intraseasonal component and interannual component during D0JFMAM1. As shown in Fig. 6a, the interannual variation of OLR is mainly distributed in the tropical WNP, corresponding to the maximum climatological precipitation center and the active area of the anomalous anticyclone/cyclone. The interannual standard deviation of OLR of the El Niño part is greater than that of the La Niña part, indicating stronger anomalous anticyclones during decay phases of warm events. During El Niño, the interannual standard deviation of OLR is predominant and considerably stronger than the intraseasonal standard deviation (Figs. 6a and c). Contrary to El Niño, the intraseasonal variation dominates the OLR standard deviation of the La Niña part (Figs. 6b and d). This is because the negative SSTAs appearing in the WNP (Fig. 2) during El Niño act to weaken the updraft branch of the Walker circulation and suppress convective activities, resulting in an adverse condition for intraseasonal oscillation activities. This hypothesis is similar to the viewpoint that positive air–sea feedback tends to sustain the WNPAC and negative air–sea feedback can work to excite or enhance the intraseasonal oscillation in the monsoon trough (Wang and Zhang, 2002; Liu and Wang, 2014). Therefore, during an El Niño mature phase the interannual variation plays the dominant role and the atmospheric variability is more energetic on the interannual time scale, which is conducive to a steady persistence of the WNPAC. Contrary to the El Niño case, the positive SSTAs during La Niña in the WNP serve to strengthen the updraft branch of the Walker circulation and enhance convective activities, and thus the WNPC cannot persist steadily because of the active intraseasonal disturbances. As the WNPC may be disturbed frequently by the intraseasonal oscillation during La Niña, the positive feedback between the WNPC and warm SSTA cannot be steadily maintained. As a result, the WNPC is unable to effectively grow, leading to a weaker equatorial zonal wind stress anomaly during La Niña mature-to-decay phases. Moreover, as the OLR anomaly during El Niño is much stronger than that during La Niña, the suppression of intraseasonal oscillation during El Niño is stronger further.

As mentioned above, the anomalous zonal winds over the equatorial WP play a crucial role in the decay of ENSO events, which is tightly associated with the WNPAC/WNPC (Wang and Fiedler, 2006). To illustrate the effect of intraseasonal oscillation on the equatorial zonal wind anomalies, we calculate the regionally averaged intraseasonal and interannual components of 850 hPa zonal wind anomalies over the equatorial WP area, and their standard deviations are shown in Fig. 7. It is clear that the interannual standard deviation of 850 hPa anomalous zonal winds is greater than the intraseasonal standard deviation during El Niño, while the opposite occurs during La Niña. Comparing the cases between El Niño and La Niña, the standard deviation of anomalous interannual zonal wind during El Niño is stronger than during La Niña, with the ratio between two phases during D0JF1 and D0JFMAM1 being about 2. The interannual standard deviation during El Niño is statistically significant above the 99% confidence level, while that during La Niña is not significant. However, the standard deviation of intraseasonal zonal wind anomalies during La Niña is larger than during El Niño, and the ratio between them during D0JF1 and D0JFMAM1 is 1.38 and 1.34, respectively. Unlike its interannual part, the intraseasonal standard variation during El Niño is not statistically significant above the 99% confidence level, while that during La Niña is significant. As the interannual and intraseasonal standard deviations represent their amplitudes, it implies that the interannual amplitude of 850 hPa zonal wind anomalies during El Niño is about twice that during La Niña, which is consistent with the results of Figs. 4 and 5. The amplitudes of the interannual and intraseasonal 850 hPa zonal wind anomalies during El Niño's D0JF1 are 1.66 and 1.19, and those during La Niña are 0.74 and 1.64, respectively, in-

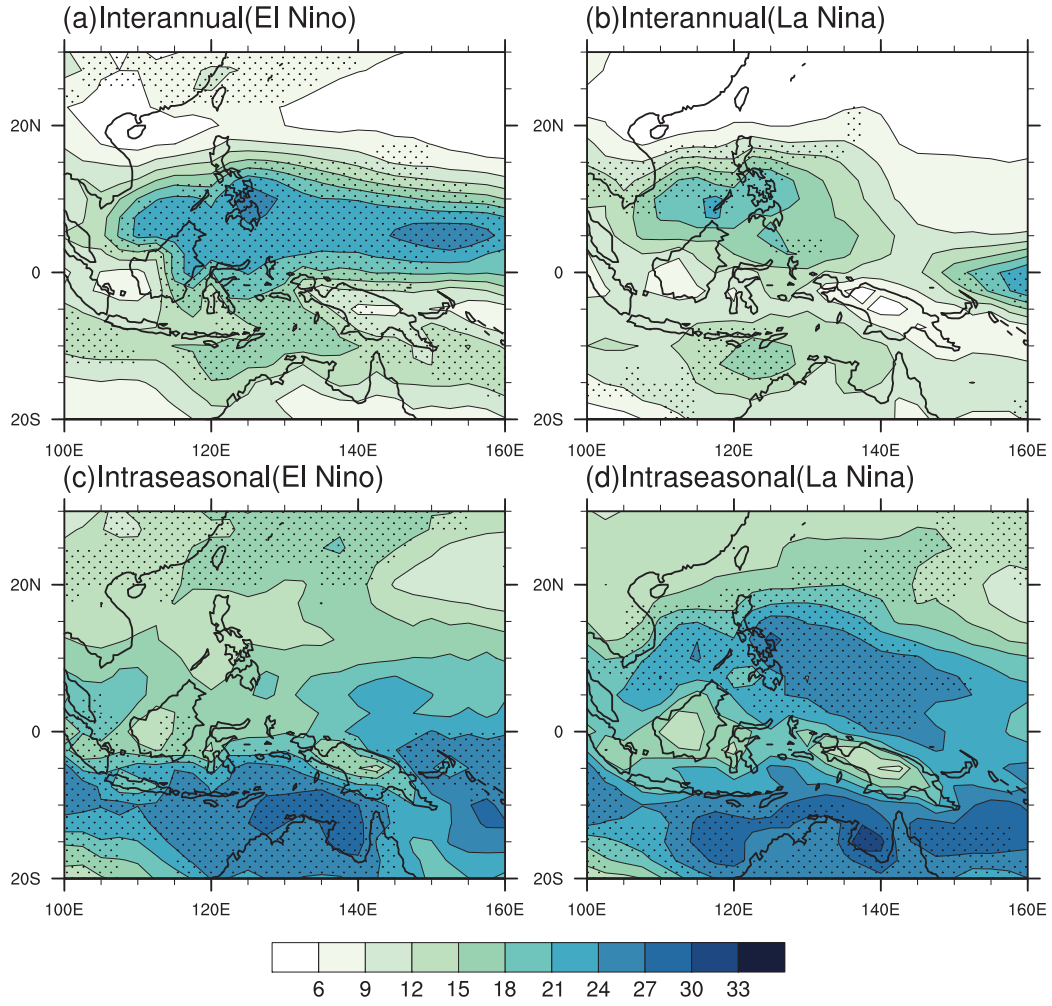

Fig. 6. Standard deviations (units: W m^{-2}) of the (a, b) interannual and (c, d) intraseasonal component of OLR for (a, c) El Niño and (b, d) La Niña during D0JFMAM1. Dotted areas are significant above the 99% confidence level.

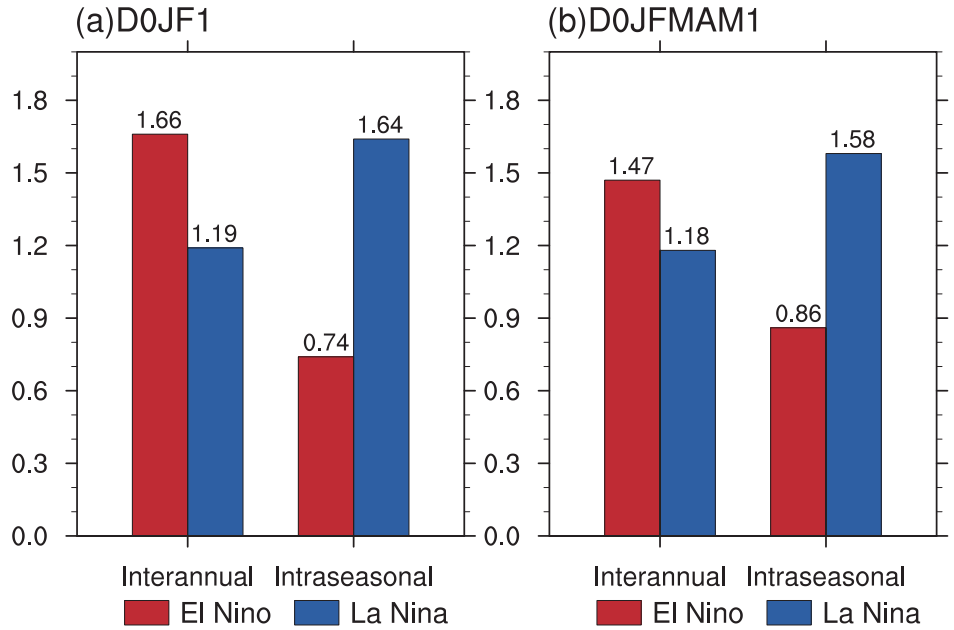

Fig. 7. Standard deviations of 850 hPa zonal wind interannual (blue) and intraseasonal (red) components for El Niño and La Niña during (a) mature phases and (b) mature-to-decay phases. The region in which the 850 hPa zonal winds are averaged is (5°S–5°N, 100°–140°E).

dicating that the sums of the interannual and intraseasonal amplitudes are roughly equal between El Niño and La Niña. In other words, the kinetic energy is approximately conserved during El Niño and La Niña. The same result can been found for D0JFMAM1. In summary, during El Niño, the suppression of convection over the tropical WNP weakens the intraseasonal oscillation, and thus the energy of the wind field is mainly concentrated on the interannual time scale, resulting in stronger interannual zonal wind anomalies; whereas, the enhanced convection during La Niña favors stronger intraseasonal oscillation, and thus the energy from the atmospheric wind field is mainly concentrated on the intraseasonal time scale, leading to a weaker zonal wind anomaly. This process therefore brings about the pronounced asymmetry of anomalous zonal wind between El Niño and La Niña over the equatorial WP, and ultimately leads to asymmetric decay speeds of El Niño and La Niña.

5. OGCM experiments

5.1. *Experimental design*

In order to quantify the effect of the asymmetric equatorial WP zonal wind anomalies on the decays of El Niño and La Niña, we conduct four sensitivity experiments, which are shown in Table 1. In the experiments, the composite zonal wind stress anomalies over the equatorial WP (15°S–15°N, 100°–160°E) during El Niño and La Niña mature phases (D0JF1) as well as mature-to-decay phases (D0JFMAM1) are superimposed onto the climatological zonal wind stress field of the control experiment. Since the difference between the control and sensitivity experiments is only the zonal wind stress forcing, the SST difference between two experiments can measure the effect of wind stress. By comparing the simulations of El Niño and La Niña anomalous zonal wind stress forcing, we can identify how the asymmetric zonal wind stress anomalies impact ENSO decay.

Figure 8 shows the composite zonal wind stress anomalies of four sensitivity experiments. In general, each of these anomalous patterns is consistent with that in Fig. 3c. The easterly anomalies are distributed around the equator and the westerly anomalies around 20°N during El Niño, and vice versa during La Niña. Notably, the easterly wind stress anomalies tend to strengthen and extend eastward with time

Table 1. Details of the sensitivity experiments.

Experiement	Superposed Zonal wind stress anomalies
EL_D0JF1	December–February of El Niño mature phase
EL_D0JFMAM1	December–May of El Niño mature-to-decay phases
LA_D0JF1	December–February of La Niña mature phase
LA_D0JFMAM1	December–May of La Niña mature-to-decay phases

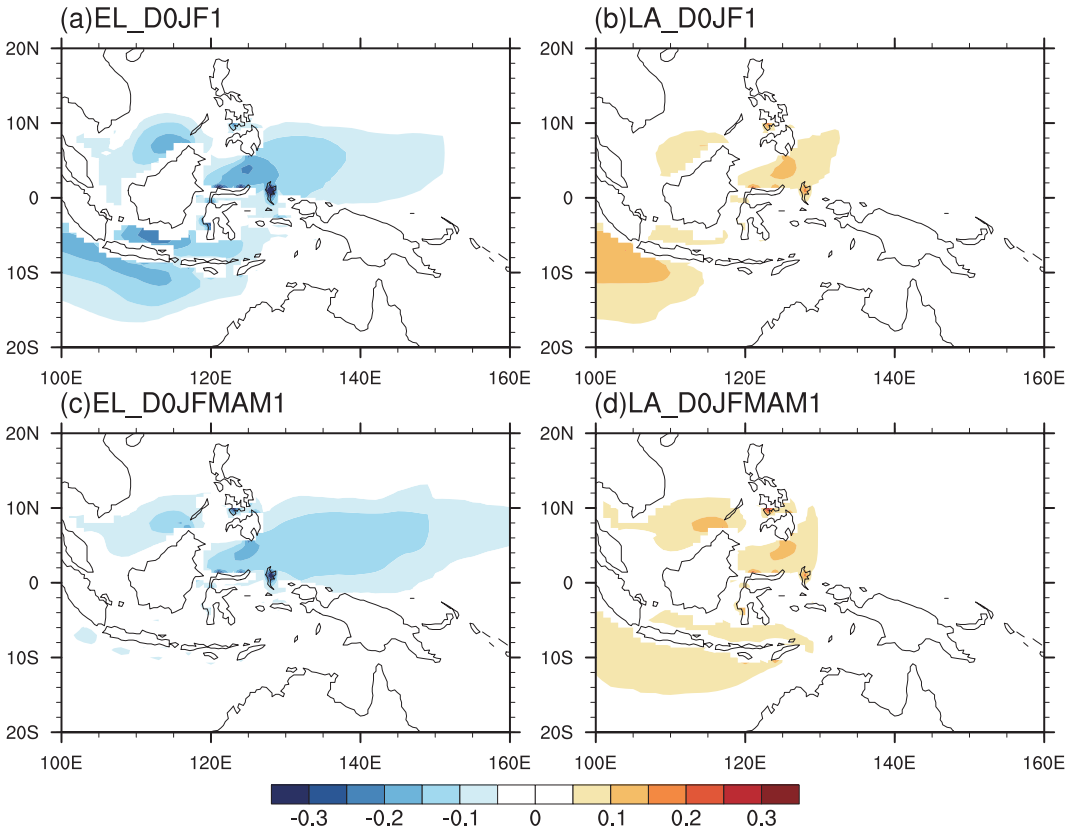

Fig. 8. Zonal wind stress anomalies superposed in sensitivity experiments for (a) EL_D0JF1, (b) LA_D0JF1, (c) EL_D0JFMAM1, and (d) LA_D0JFMAM1.

during El Niño, while the westerly wind stress anomalies during La Niña show little change, in agreement with the results in Fig. 2.

5.2. *Effect of anomalous zonal wind stress on SST*

Figure 9 displays the differences in Niño3 index between the four sensitivity experiments and the control experiment, which represents the influence of anomalous zonal wind stress on ENSO decay. For the convenience of comparison, the results of EL_D0JF1 and EL_D0JFMAM1 are multiplied by −1. As shown in Fig. 9, the SSTAs over CEEP become visible from the following March after the ENSO peak phase. The negative SSTAs that arise over CEEP correspond to the easterly wind stress anomalies over the equatorial WP during El Niño, while westerly wind stress anomalies result in positive SSTAs during La Niña. Because easterly (westerly) anomalies over the equatorial WP during El Niño (La Niña) can stimulate cold (warm) Kelvin waves, the warm (cold) SSTA over CEEP will be declined by eastward propagating cold (warm) Kelvin waves (Zhang and Huang, 1998; Wang and Fiedler, 2006). The eastward propagation of Kelvin waves can be seen clearly from the equatorial longitude–time sections of upper-ocean HC (Fig. 10). Negative HC anomalies propagate eastward from the equatorial WP after the December of an El Niño mature phase and arrive at the eastern boundary of the ocean in the following February when the SSTAs over CEEP (Niño3 index) begin to be noticeable. The speed of HC propagation is approximately equivalent to the speed of equatorial Kelvin waves (Fig. 9). Conversely, positive HC anomalies propagate eastward during La Niña. The strongest HC anomalies appear around the equatorial EP in the May–June during a decaying El Niño, when SSTAs peak too. The same results can been found during La Niña (Fig. 9).

The SSTAs simulated by the sensitivity experiments show features consistent with observations insofar as evident asymmetry exists between El Niño and La Niña. The maxima of Niño3 index anomalies of EL_D0JF1 and EL_D0JFMAM1 are −0.18°C and −0.26°C, respectively; while those of LA_D0JF1 and LA_D0JFMAM1 are only 0.06°C and 0.08°C (Fig. 9), respectively. The negative SSTAs in the Niño3 region induced by the equatorial WP easterly wind stress

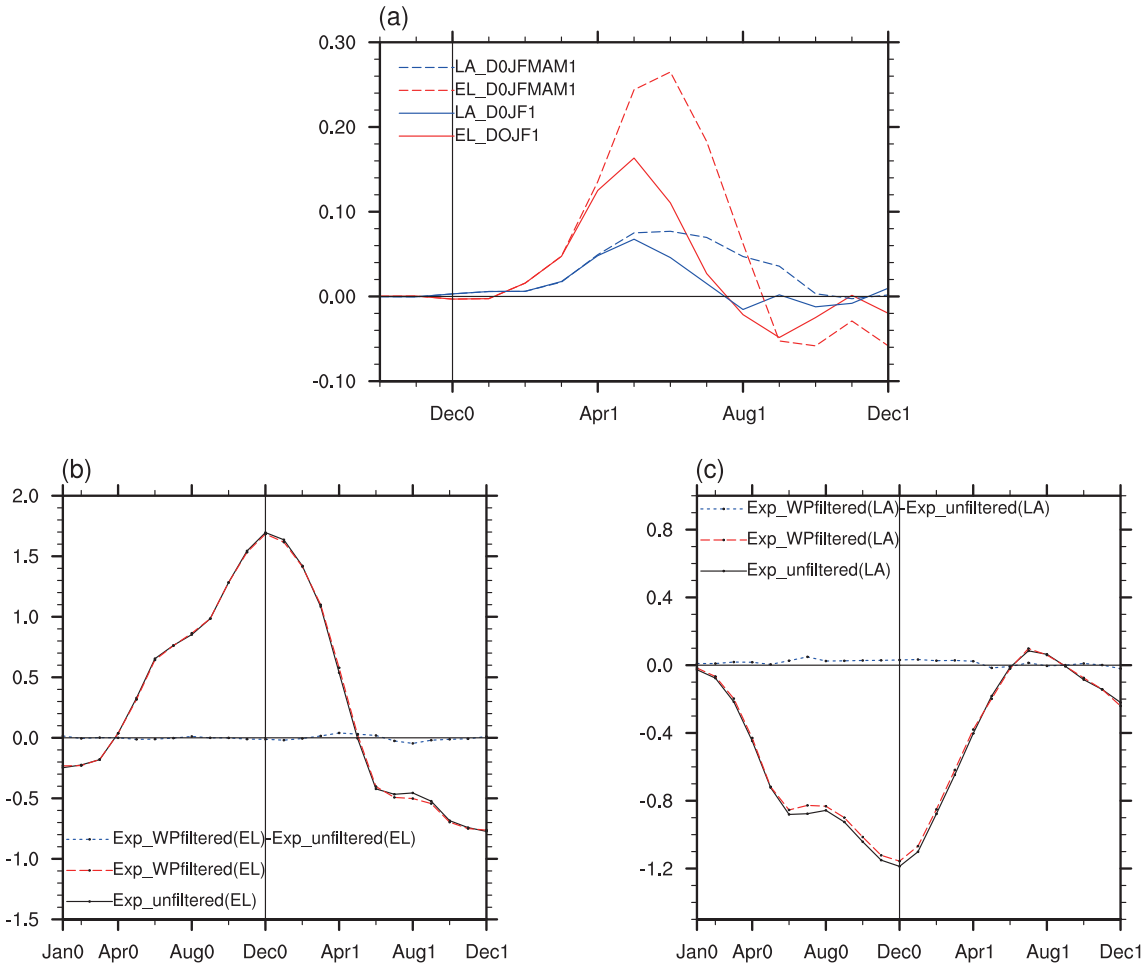

Fig. 9. (a) Time series of Niño3 index differences between the control and sensitivity experiments (units: °C). (b, c) Composite Niño3 index derived from the Exp_unfiltered (black lines) and Exp_WPfiltered (red lines) experiments for El Niño and La Niña, respectively. The differences between Exp_unfiltered and Exp_WPfiltered are denoted by blue lines.

anomalies during El Niño are threefold greater than the positive SSTAs induced by westerly wind stress anomalies during La Niña. Significant asymmetric characteristics can also be observed in oceanic HC anomalies, with the HC anomalies of the upper 400 m during El Niño being four to five times as large as those during La Niña (Fig. 10). The asymmetry in SSTAs and HC anomalies correspond well to the asymmetry of wind stress. Both the intensity and extension of the easterly wind stress anomalies during El Niño are notably greater than those of westerly wind stress anomalies during La Niña (Fig. 8), and these asymmetries are stronger than the asymmetry of 850 hPa zonal winds. Accordingly, it is favorable for El Niño to decay faster, while the cold SSTAs during La Niña tend to maintain for a longer period. Noting that there is some evident HC signal near 140°W, such a signal may be associated with the tropical instability waves.

5.3. *Impact of intraseasonal wind stress anomalies on ENSO*

Previous studies suggest that the atmospheric intraseasonal variation rectifies the interannual oceanic variation via nonlinear ocean processes (Kessler and Kleeman, 2000; Rong et al., 2011; Zhao et al., 2019). To investigate the contribution of this oceanic route by which the atmospheric intraseasonal oscillation impacts ENSO decay, we conduct two additional numerical experiments. In the Exp_unfiltered experiment, the original unfiltered daily wind stress anomalies from 1979 to 2016 are used to force the model, whereas in the Exp_WPfiltered experiment a 90-day running mean is applied to daily wind stress anomalies over the tropical WP (20°S–20°N, 100°E–160°W). Figures 9b and c show the composite Niño3 indexes and differences between Exp_unfiltered and Exp_WPfiltered during El Niña and La Niña, respectively. It

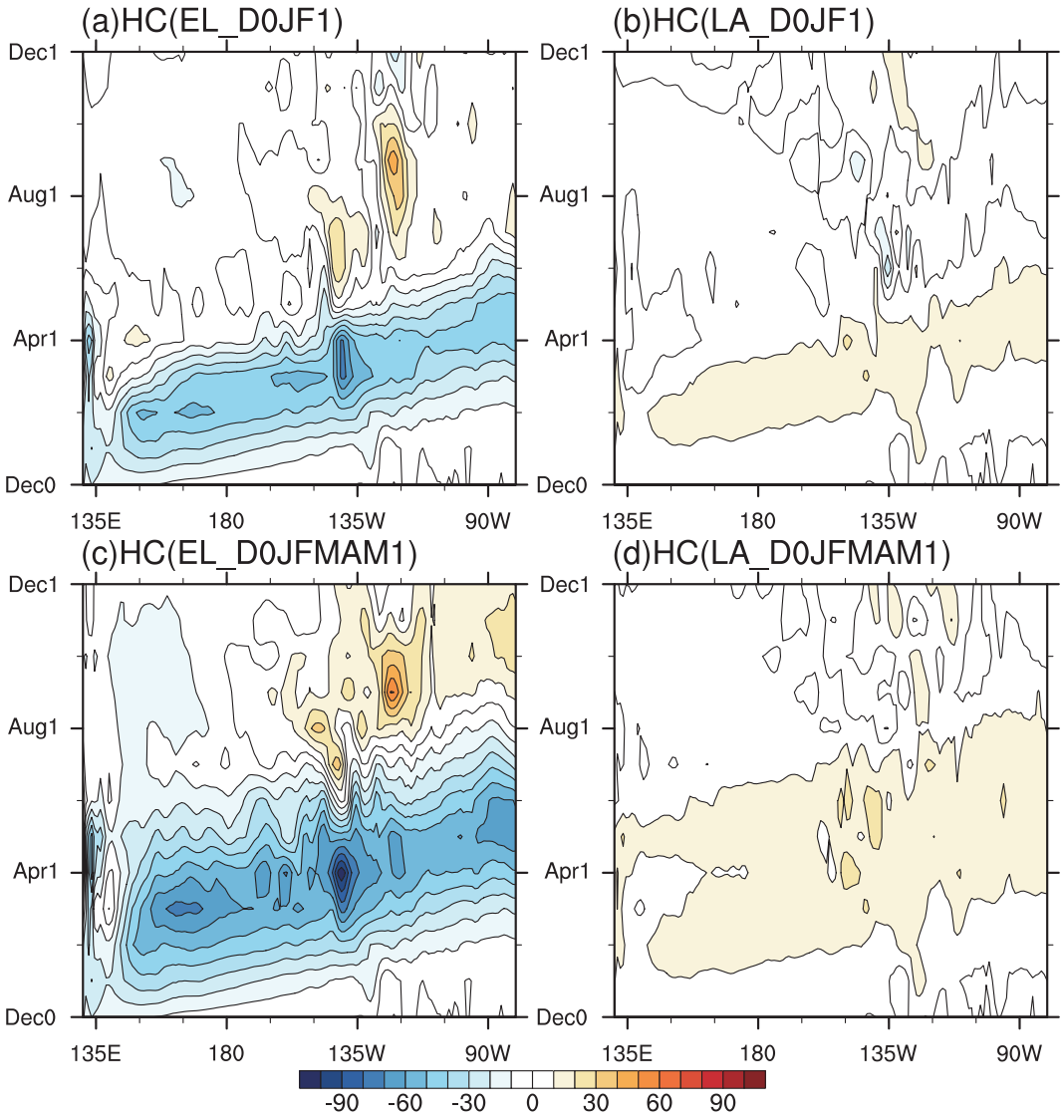

Fig. 10. Simulated longitude–time cross sections of equatorial (averaged over 5°S–5°N) upper ocean HC differences between the control and sensitivity experiments for (a) EL_D0JF1, (b) LA_D0JF1, (c) EL_D0JFMAM1, and (d) LA_D0JFMAM1. The HC is defined as the vertical integration of temperature by depth from the ocean surface to 400 m (units: °C m^{-1}).

can be seen that both the Exp_unfiltered and Exp_WPfiltered experiments reproduce the observed Niño3 indexes for El Niño and La Niña well. However, the atmospheric intraseasonal wind stress anomalies exhibit a very limited effect on the decay of both El Niño and La Niña, with the Niño3 index being almost unchanged between Exp_unfiltered and Exp_WPfiltered for both warm and cold events. This result is consistent with the simulations of Rong et al. (2011) and Zhao et al. (2019), who used different OGCMs to investigate the rectifications of the intraseasonal wind stress on the interannual oceanic variability. Their studies also showed limited-amplitude and small-scale ocean SSTAs in response to the intraseasonal wind stress anomalies. Thus, the above experiments indicate that the effect of intraseasonal wind stress anomalies on ENSO decay is negligible.

6. Conclusion and discussion

The analyses of observational data in this paper show that the decay speed of El Niño is larger than that of La Niña, indicating significant asymmetry in this respect between them. In order to explore the physical mechanism causing this asymmetry, we analyze the anomalous features of SST and atmospheric circulation over the WNP during El Niño and La Niña mature-to-decay phases. It is revealed that the magnitudes of SST, 850 hPa wind, and SLP anomalies over the tropical WNP during El Niño are all greater than those during La Niña, indicating that remarkable asymmetries exist in these fields too.

The OLR and equatorial zonal wind anomalies show significantly stronger interannual standard deviations than their intraseasonal standard deviations over the tropical WP during El Niño mature-to-decay phases; however, during La Niña the intraseasonal standard deviations are larger than the interannual standard deviations. It seems that the suppressed convection during El Niño is able to weaken the intraseasonal oscillation and, as a result, the atmospheric wind anomalies are more energetic on the interannual timescale; whereas, during La Niña the enhanced convection tends to strengthen the intraseasonal oscillation, and the atmosphere obtains most of its kinetic energy through intraseasonal variation, leading to a weakened interannual fluctuation. Therefore, the difference in intraseasonal oscillation intensity may play an important role in strengthening the asymmetry of zonal wind anomalies over the equatorial WP during El Niño and La Niña decay phases.

Numerical experiments show that the asymmetric zonal wind stress anomalies during El Niño and La Niña decay phases can induce asymmetry in SSTA decay speeds over CEEP by exciting different equatorial Kelvin waves. The maximum negative anomalies of Niño3 index induced by the zonal wind stress anomalies during El Niño mature phases (D0JF1) and mature-to-decay (D0JFMAM1) phases are −0.18°C and −0.26°C, respectively, which are threefold greater than the positive Niño3 index during La Niña, indicating that the stronger zonal wind anomalies over the equatorial WP favor a faster decay of El Niño. The numerical experiments also show that the intraseasonal wind stress anomalies have negligible impact on ENSO decay. Furthermore, we demonstrate that the initial state of the evolving ocean is an important component of interannual variability. However, using the initial state with regard to El Niño or La Niña may contain additional signals of other processes or forcings—for instance, the reflection of the off-equatorial Rossby waves in the equatorial WP. Moreover, as we use the composite wind stress anomalies to force the sensitivity experiments, it is difficult to select an appropriate initial state with regard to El Niño and La Niña, since we cannot use a composite initial state, which is generally dynamically unbalanced.

Nevertheless, it should be pointed out that the Niño3 index induced by the zonal wind stress anomalies in the four sensitivity experiments are all less than 0.3°C (Fig. 9); however, as shown in Fig. 1, the observational Niño3 index during both El Niño and La Niña exceeds 1°C. That is, despite the zonal wind anomalies over the equatorial WP being favorable to asymmetric ENSO decay, there might be additional processes that contribute to ENSO decay too. The relative contributions of other processes and zonal wind anomalies over the equatorial WP to ENSO asymmetric decay require further exploration.

Acknowledgements. This study was supported by the China National 973 Project (Grant No. 2015CB453203), the National Key R&D Program of China (Grant No. 2016YFA0600602), and the National Natural Science Foundation of China (Grant No. 41661144017).

REFERENCES

Abellán, E., and S. McGregor, 2016: The role of the southward wind shift in both, the seasonal synchronization and duration of ENSO events. *Climate Dyn.*, **47**(1–2), 509–527, https://doi.org/10.1007/s00382-015-2853-1.

An, S.-I., 2008: Interannual variations of the tropical ocean instability wave and ENSO. *J. Climate*, **21**(15), 3680–3686, https://doi.org/10.1175/2008JCLI1701.1.

An, S.-I., and F.-F. Jin, 2004: Nonlinearity and asymmetry of ENSO. *J. Climate*, **17**, 2399–2412, https://doi.org/10.1175/1520-0442(2004)017<2399:NAAOE>2.0.CO;2.

Battisti, D. S., and A. C. Hirst, 1989: Interannual variability in a tropical atmosphere-ocean model: Influence of the basic state, ocean geometry and nonlinearity. *J. Atmos. Sci.*, **46**, 1687–1712, https://doi.org/10.1175/1520-0469(1989)046<1687:IVIATA>2.0.CO;2.

Chen, M. C., T. Li, X. Y. Shen, and B. Wu, 2016: Relative roles of dynamic and thermodynamic processes in causing evolution asymmetry between El Niño and La Niña. *J. Climate*, **29**(6), 2201–2220, https://doi.org/10.1175/JCLI-D-15-0547.1.

Da Silva, A. M., C. C. Young, and S. Levitus, 1994: Atlas of surface marine data 1994. Vol. 2, Anomalies of directly observed quantities. NOAA Atlas NESDIS 7, 416 pp.

Dee, D. P., and Coauthors, 2011: The ERA-interim reanalysis: Configuration and performance of the data assimilation system. *Quart. J. Roy. Meteor. Soc.*, **137**(656), 553–597, https://doi.org/10.1002/qj.828.

DiNezio, P. N., and C. Deser, 2014: Nonlinear controls on the persistence of La Niña. *J. Climate*, **27**(19), 7335–7355, https://doi.org/10.1175/JCLI-D-14-00033.1.

Dommenget, D., T. Bayr, and C. Frauen, 2013: Analysis of the non-linearity in the pattern and time evolution of El Niño Southern Oscillation. *Climate Dyn*., **40**, 2825–2847, https://doi.org/10.1007/s00382-012-1475-0.

Gao, R. L., R. H. Zhang, M. Wen, and T. R. Li, 2018: Interdecadal changes in the asymmetric impacts of ENSO on wintertime rainfall over china and atmospheric circulations over western north pacific. *Climate Dyn*., in press, https://doi.org/10.1007/s00382-018-4282-4.

Harrison, D. E., and G. A. Vecchi, 1999: On the termination of El Niño. *Geophys. Res. Lett*., **26**, 1593–1596, https://doi.org/10.1029/1999GL900316.

Hoerling, M. P., A. Kumar, and M. Zhong, 1997: El Niño, La Niña, and the nonlinearity of their teleconnections. *J. Climate*, **10**, 1769–1786, https://doi.org/10.1175/1520-0442(1997)010<1769:ENOLNA>2.0.CO;2.

Hu, Z. Z., A. Kumar, Y. Xue, and B. Jha, 2014: Why were some La Niñas followed by another La Niña? *Climate Dyn*., **42**(3–4), 1029–1042, https://doi.org/10.1007/s00382-013-1917-3.

Huang, R. H., R. H. Zhang, and B. L. Yan, 2001: Dynamical effect of the zonal wind anomalies over the tropical western Pacific on ENSO cycles. *Science in China Series D*: *Earth Sciences*, **44**(12), 1089–1098, https://doi.org/10.1007/BF02906865.

Jin, E. K., and J. L. Kinter III, 2009: Characteristics of tropical Pacific SST predictability in coupled GCM forecasts using the NCEP CFS. *Climate Dyn*., **32**(5), 675–691, https://doi.org/10.1007/s00382-008-0418-2.

Jin, F.-F., 1997: An equatorial ocean recharge paradigm for ENSO. Part I: Conceptual mode. *J. Atmos. Sci*., **54**, 811–829, https://doi.org/10.1175/1520-0469(1997)054<0811:AEORPF>2.0.CO;2.

Kang, I.-S., and J.-S. Kug, 2002: El Niño and La Niña sea surface temperature anomalies: Asymmetry characteristics associated with their wind stress anomalies. *J. Geophys. Res*., **107**, 4372, https://doi.org/10.1029/2001JD000393.

Kessler, W. S., 2002: Is ENSO a cycle or a series of events? *Geophys. Res. Lett*., **29**, 2125, https://doi.org/10.1029/2002GL015924.

Kessler, W. S., and R. Kleeman, 2000: Rectification of the Madden-Julian oscillation into the ENSO cycle. *J. Climate*, **13**(20), 3560–3575, https://doi.org/10.1175/1520-0442(2000)013<3560:ROTMJO>2.0.CO;2.

Larkin, N. K., and D. E. Harrison, 2002: ENSO warm (El Niño) and cold (La Niña) event life cycles: Ocean surface anomaly patterns, their symmetries, asymmetries, and implications. *J. Climate*, **15**, 1118–1140, https://doi.org/10.1175/1520-0442(2002)015<1118:EWENOA>2.0.CO;2.

Levitus, S, 1982: Climatological atlas of the world ocean. NOAA Professional Paper 13.

Li, T., B. Wang, B. Wu, T. J. Zhou, C.-P. Chang, and R. H. Zhang, 2017: Theories on formation of an anomalous anticyclone in western North Pacific during El Niño: A review. *J. Meteor. Res*., **31**, 987–1006, https://doi.org/10.1007/s13351-017-7147-6.

Li, T. R., R. H. Zhang, and M. Wen, 2015: Impact of ENSO on the precipitation over China in winter half-years. *Journal of Tropical Meteorology*, **21**, 161–170.

Liebmann, B., and C. A. Smith, 1996: Description of a complete (interpolated) outgoing longwave radiation dataset. *Bull. Amer. Meteor. Soc*., **77**, 1275–1277.

Liu F., and B. Wang, 2014: A mechanism for explaining the maximum intraseasonal oscillation center over the Western North Pacific. *J. Climate*, **27**, 958–968, https://doi.org/10.1175/JCLI-D-12-00797.1.

McGregor, S., A. Timmermann, N. Schneider, M. F. Stuecker, and M. H. England, 2012: The effect of the South Pacific convergence zone on the termination of El Niño events and the meridional asymmetry of ENSO. *J. Climate*, **25**(16), 5566–5586, https://doi.org/10.1175/JCLI-D-11-00332.1.

McPhaden, M. J., and X. B. Zhang, 2009: Asymmetry in zonal phase propagation of ENSO sea surface temperature anomalies. *Geophys. Res. Lett*., **36**, L13703, https://doi.org/10.1029/2009GL038774.

Nagura, M., K. Ando, and K. Mizuno, 2008: Pausing of the ENSO cycle: A case study from 1998 to 2002. *J. Climate*, **21**, 342–363, https://doi.org/10.1175/2007JCLI1765.1.

Ohba, M., and H. Ueda, 2009: Role of nonlinear atmospheric response to SST on the asymmetric transition process of ENSO. *J. Climate*, **22**, 177–192, https://doi.org/10.1175/2008JCLI2334.1.

Ohba, M., and M. Watanabe, 2012: Role of the Indo-Pacific interbasin coupling in predicting asymmetric ENSO transition and duration. *J. Climate*, **25**(9), 3321–3335, https://doi.org/10.1175/JCLI-D-11-00409.1.

Okumura, Y. M., and C. Deser, 2010: Asymmetry in the duration of El Niño and La Niña. *J. Climate*, **23**, 5826–5843, https://doi.org/10.1175/2010JCLI3592.1.

Okumura, Y. M., M. Ohba, C. Deser, and H. Ueda, 2011: A proposed mechanism for the asymmetric duration of El Niño and La Niña. *J. Climate*, **24**, 3822–3829, https://doi.org/10.1175/2011JCLI3999.1.

Pacanowski, R. C., and S. M. Griffies, 1999: MOM 3.0 Manual. NOAA/Geophysical Fluid Dynamics. Laboratory, Princeton, NJ, 668 pp.

Rayner, N. A., D. E. Parker, E. B. Horton, C. K. Folland, L. V. Alexander, D. P. Rowell, E. C. Kent, and A. Kaplan, 2003: Global analyses of sea surface temperature, sea ice, and night marine air temperature since the late nineteenth century. *J. Geophys. Res*., **108**, 4407, https://doi.org/10.1029/2002JD002670.

Rong, X. Y., R. H. Zhang, T. Li, and J. Z. Su, 2011: Upscale feedback of high-frequency winds to ENSO. *Quart. J. Roy. Meteor. Soc*., **137**(657), 894–907, https://doi.org/10.1002/qj.804.

Su, J. Z., R. H. Zhang, T. Li, X. Y. Rong, J.-S. Kug, and C.-C. Hong, 2010: Causes of the El Niño and La Niña amplitude asymmetry in the equatorial eastern Pacific. *J. Climate*, **23**, 605–617, https://doi.org/10.1175/2009JCLI2894.1.

Suarez, M. J., and P. S. Schopf, 1988: A delayed action oscillator for ENSO. *J. Atmos. Sci*., **45**, 3283–3287, https://doi.org/10.1175/1520-0469(1988)045<3283:ADAOFE>2.0.CO;2.

Tao, W. C., Huang, G., Wu, R. G., Hu, K. M., Wang, P. F., and Chen, D, 2017: Asymmetry in summertime atmospheric circulation anomalies over the northwest Pacific during decaying phase of El Niño and La Niña. *Climate Dyn*., **49**(5–6), 2007–2023, https://doi.org/10.1007/s00382-016-3432-9.

Timmermann, A., and F. F. Jin, 2002: A nonlinear mechanism for decadal El Niño amplitude changes. *Geophys. Res. Lett*., **29**(1), 1003, https://doi.org/10.1029/2001GL013369.

Tokinaga, H., S.-P. Xie, C. Deser, Y. Kosaka, and Y. M. Okumura, 2012: Slowdown of the Walker circulation driven by tropical Indo-Pacific warming. *Nature*, **491**, 439–443, https://doi.org/

10.1038/nature11576.

Wang, B., and Q. Zhang, 2002: Pacific-East Asian teleconnection. Part II: How the Philippine Sea anomalous anticyclone is established during El Niño development. *J. Climate*, **15**, 3252–3265, https://doi.org/10.1175/1520-0442(2002)015<3252:PEATPI>2.0.CO;2.

Wang, B., R. G. Wu, and X. H. Fu, 2000: Pacific-East Asian teleconnection: How does ENSO affect East Asian climate? *J. Climate*, **13**, 1517–1536, https://doi.org/10.1175/1520-0442(2000)013<1517:PEATHD>2.0.CO;2.

Wang, C. Z., and P. C. Fiedler, 2006: ENSO variability and the eastern tropical Pacific: A review. *Progress in Oceanography*, **69**(2–4), 239–266.

Wang, C. Z., R. H. Weisberg, and J. I. Virmani, 1999: Western Pacific interannual variability associated with the El Niño–Southern Oscillation. *J. Geophys. Res.*, **104**, 5131–5149, https://doi.org/10.1029/1998JC900090.

Wu, B., T. Li, and T. J. Zhou, 2010: Asymmetry of atmospheric circulation anomalies over the western North Pacific between El Niño and La Niña. *J. Climate*, **23**, 4807–4822, https://doi.org/10.1175/2010JCLI3222.1.

Xie, S. P., K. M. Hu, J. Hafner, H. Tokinaga, Y. Du, G. Huang, and T. Sampe, 2009: Indian Ocean capacitor effect on indo-western Pacific climate during the summer following El Niño. *J. Climate*, **22**(3), 730–747, https://doi.org/10.1175/2008JCLI2544.1.

Yan, B. L., R. H. Huang, and R. H. Zhang, 2001: Dynamical role of zonal wind stresses over the tropical pacific in the occurring and vanishing of El Niño Part II: Analyses of modeling results. *Chinese Journal of Atmospheric Sciences*, **25**(2), 160–172, https://doi.org/10.3878/j.issn.1006-9895.2001.02.02. (in Chinese)

Zhang, R. H., and R. H. Huang, 1998: Dynamical roles of zonal wind stresses over the tropical Pacific on the occurring and vanishing of El Niño. Part I: Diagnostic and theoretical analyses. *Chinese Journal of Atmospheric Sciences*, **22**(4), 587–599, https://doi.org/10.3878/j.issn.1006-9895.1998.04.19. (in Chinese)

Zhang, R. H., A. Sumi, and M. Kimoto, 1996: Impact of El Niño on the East Asian monsoon: A diagnostic study of the '86/87 and '91/92 events. *J. Meteor. Soc. Japan*, **74**, 49–62, https://doi.org/10.2151/jmsj1965.74.1_49.

Zhang, R. H., T. R. Li, M. Wen, and L. K. Liu, 2015: Role of intraseasonal oscillation in asymmetric impacts of El Niño and La Niña on the rainfall over southern China in boreal winter. *Climate Dyn.*, **45**(3–4), 559–567, https://doi.org/10.1007/s00382-014-2207-4.

Zhang, R. H., Q. Y. Min, and J. Z. Su, 2017: Impact of El Niño on atmospheric circulations over East Asia and rainfall in China: Role of the anomalous western North Pacific anticyclone. *Science China Earth Sciences*, **60**, 1124–1132, https://doi.org/10.1007/s11430-016-9026-x.

Zhao, X., D. L. Yuan, G. Yang, J. Wang, H. L. Liu, R. H. Zhang, and W. Q. Han, 2019: Interannual variability and dynamics of intraseasonal wind rectification in the equatorial Pacific Ocean. *Climate Dyn.*, **52**, 4351–4369, https://doi.org/10.1007/s00382-018-4383-0.